

# A semi-classical approach to electron spin resonance in quantum spin systems

Shunsuke C. Furuya and Masaki Oshikawa

*Institute for Solid State Physics, University of Tokyo, Kashiwa 277-8581, Japan*

Ian Affleck

*Department of Physics and Astronomy, University of British Columbia, Vancouver, BC, Canada V6T 1Z1*

(Dated: December 3, 2018)

We develop a semi-classical approximation to electron spin resonance in quantum spin systems, based on the rotor or non-linear sigma model. The classical time evolution is studied using molecular dynamics while random initial conditions are sampled using classical Monte Carlo methods. Although the approximation may be especially powerful in two dimensions, we apply it here to one-dimensional systems of large spin at intermediate temperatures, in the presence of staggered and uniform magnetic fields. We first test the validity of the semi-classical approximation by comparing the magnetization to quantum Monte Carlo results on  $S = 2$  chains. Then we calculate the ESR spectrum, finding broad coexisting paramagnetic and spin wave resonances.

PACS numbers: 76.20.+q, 75.10.Pq, 03.65.Sq

## I. INTRODUCTION

Electron spin resonance probes the dynamics of interacting spin systems at zero wave-vector in a magnetic field. The intensity of adsorption of microwave radiation of frequency  $\omega$  is  $\propto \omega G_{\alpha\alpha}^R(\omega)$  where  $G_{\alpha\alpha}^R(\omega)$  is the retarded Green's function of  $S_T^\alpha \equiv \sum_r S_r^\alpha$ , the  $\alpha$  component of the total spin operator. Since  $[S_T^\alpha, H_0] = 0$  for an SU(2) invariant Hamiltonian,  $H_0$ , such as the Heisenberg model, the ESR spectrum remains exactly the same as that for a single spin. Thus ESR is a highly sensitive probe to small anisotropies in the Hamiltonian. In order to discuss the effect of small anisotropies, the calculation of ESR spectra has to be very precise. An approximation, that may be reasonable to study other properties such as inelastic neutron scattering spectrum, might lead to an erroneous change of ESR, even in the absence of anisotropy. Then it could not be applied to ESR. This is a challenging aspect of ESR theory, especially in strongly correlated systems.

Older theories of ESR<sup>1,2</sup> are based on high temperature expansions at  $T \gg J$ , the exchange coupling, where each spin behaves approximately independently or else on spin-wave theory at  $T < T_N$ , the Néel temperature, typically of order  $J$ . For the two dimensional Heisenberg model on the square lattice,  $T_N = 0$ , leaving a large temperature range where neither of these approaches to ESR applies. In this “renormalized classical region” an approach to dynamics was developed by Chakravarty, Halperin and Nelson<sup>3</sup> (CHN) based on the two dimensional classical rotor model (CRM). The CRM is defined with two vector variables  $\mathbf{n}_i$  and  $\mathbf{L}_i$  at each site, and the Hamiltonian

$$\mathcal{H} = -b^{D-2} \rho_s \sum_{\langle i,j \rangle} \mathbf{n}_i \cdot \mathbf{n}_j + \frac{b^D}{2\chi_{u\perp}} \sum_i \mathbf{L}_i^2, \quad (1)$$

where  $D$  is the dimension of the lattice ( $D = 2$  in Ref. 3) and  $b$  is the lattice constant.  $\mathbf{n}_i$  and  $\mathbf{L}_j$  are subject to

constraints

$$\mathbf{n}_i^2 = 1, \quad (2)$$

$$\mathbf{n}_i \cdot \mathbf{L}_i = 0. \quad (3)$$

Physically,  $\mathbf{L}_i$  represents the angular momentum of the rotor  $\mathbf{n}_i$ , and the two parameters  $\rho_s$  and  $\chi_{u\perp}$  represent, respectively, the spin stiffness and the transverse component of uniform susceptibility.

The dynamics of the system is defined by the Hamiltonian (1) together with the Poisson brackets

$$\begin{aligned} \{L_i^\alpha, L_j^\beta\} &= \sum_\gamma \epsilon^{\alpha\beta\gamma} \delta_{ij} L_i^\gamma, \\ \{L_i^\alpha, n_j^\beta\} &= \sum_\gamma \epsilon^{\alpha\beta\gamma} \delta_{ij} n_i^\gamma, \\ \{n_i^\alpha, n_j^\beta\} &= 0, \end{aligned} \quad (4)$$

where  $\alpha, \beta, \gamma = 1, 2, 3$  and  $\epsilon^{\alpha\beta\gamma}$  is the Levi-Civita symbol.

The classical time evolution is calculated using molecular dynamics simulations starting from random initial conditions which are generated with classical Monte Carlo methods. CHN and Tyč, Chakravarty and Halperin<sup>4</sup> applied this method to calculate the neutron scattering cross-section at wave-vector near the antiferromagnetic point  $(\pi/a, \pi/a)$ , where  $a$  is the lattice constant of the spin system. The purpose of this paper is to explore the applicability of this method to dynamics at zero wave-vector, which is relevant to ESR.

In fact, as shown in Refs. 5 and 6, this classical method can also be applied in dimension  $D = 1$ , at least for sufficiently large spin magnitude,  $S$ . While Néel order doesn't occur even at  $T = 0$  for the one dimensional Heisenberg model there is another important characteristic low energy scale,  $\Delta$  of order

$$\Delta \approx J e^{-\pi S}. \quad (5)$$

For integer  $S$  this is the energy of the gapped triplet magnons, predicted by Haldane and following from the

behavior of the quantum  $O(3)$  non-linear sigma model (NLSM), basically the continuum limit of Eq. (1). At low temperatures,  $T \ll \Delta$  ESR can be calculated<sup>7,8</sup> from transitions between single magnon states (or, if appropriate symmetry breaking is included in  $H$ , from magnon production processes). Magnon-magnon interactions become unimportant in this temperature range because the magnons are dilute, with density  $\propto e^{-\Delta/T}$ . Instead, at higher temperature, the magnons are dense, and the NLSM behaves rather classically. The rotor model is nothing but a lattice version of the NLSM; thus CRM describes the classical dynamics of the NLSM.

The present approach to ESR based on the CRM can be used in the intermediate temperature range

$$\Delta \ll T \ll JS^2, \quad (6)$$

where the magnons are dense and the CRM is still valid as an effective theory. Unfortunately, this temperature range may not exist for the spin  $S = 1$  chain, for which the Haldane gap is known to be  $\Delta \sim 0.41J$ . However, the gap becomes smaller for higher  $S$  as in eq. (5) and the temperature range (6) becomes well-defined for higher spins, perhaps starting at  $S = 2$ , for which the Haldane gap is already as small<sup>9</sup> as  $\Delta \sim 0.089J$ .

While the classical method has a wider range of  $T$  and  $S$  over which it is applicable in  $D = 2$ , we focus on the  $D = 1$  case in this paper, due to the computational cost of the classical technique, which appears to be quite severe for ESR studies. We hope to return to the  $D = 2$  case in the future. Therefore, in this paper, we discuss ESR in 1D systems in the previously unexplored temperature regime (6). We will discuss conditions for the present approach to be applicable, in more detail, in Sec. III A.

Following Refs. 4 and 6, initial states are generated by classical Monte Carlo simulation of the  $O(3)$  CRM at given temperature. The real-time correlation function is then obtained by solving the classical equation of motion for the  $O(3)$  CRM with the initial condition. ESR spectrum can be obtained from Fourier transform of the real-time correlation function.

Among various possible anisotropies, in this paper we discuss the staggered field, which is known to have most interesting effects on ESR spectra in  $S = 1/2$  and  $S = 1$  cases. The effective Hamiltonian including the staggered field is given by

$$\mathcal{H} = \sum_j J \mathbf{S}_j \cdot \mathbf{S}_{j+1} - HS_j^z - (-1)^j h S_j^x, \quad (7)$$

where  $H$  and  $h$  is the uniform field and the transverse staggered field respectively. Throughout this paper, we set  $g\mu_B = \hbar = k_B = 1$  for simplicity.

While the staggered field might seem unphysical, it often does appear effectively in actual quantum antiferromagnetic chains. When an external magnetic field is applied to a material with a staggered crystal structure along the chain, the staggered field is effectively generated through a staggered  $g$  tensor<sup>10,11</sup> and also through

a staggered Dzyaloshinskii-Moriya interaction.<sup>12</sup> Examples of such materials include the typical  $S = 1$  Haldane chain material  $\text{Ni}(\text{C}_2\text{H}_8\text{N}_2)_2\text{NO}_2\text{ClO}_4$  (NENP)<sup>13</sup>, and the  $S = 1/2$  Heisenberg antiferromagnetic chain  $\text{Cu benzoate}$ <sup>14</sup>.

For ESR in the  $S = 1/2$  antiferromagnetic chain at low temperatures, field theory approach leads to diverging linewidth of the paramagnetic peak at lower temperatures, and an appearance of a new peak when the temperature is lowered further down to zero<sup>15,16</sup>. For ESR in the  $S = 1$  Haldane chain at low temperatures, the violation of selection rule by the staggered field leads to the appearance of a new peak at the frequency equal to the Haldane gap, corresponding to creation of a single magnon<sup>10,11</sup>. These approaches are only justified in a “quantum” regime and no longer valid for a Haldane chain at the intermediate temperatures (6), which is the focus of the present paper.

The  $S = 2$  Heisenberg antiferromagnetic chain, for which the present approach would be relevant, is not just a theoretical toy model. Granroth *et al.*<sup>17</sup> reported an experimental evidence of Haldane gap in an  $S = 2$  antiferromagnetic Heisenberg chain compound  $\text{MnCl}_3(\text{bpy})$  (bpy = bipyridine).  $\text{MnCl}_3(\text{bpy})$  is similar to NENP. It has a quite small single ion anisotropy  $D/J \leq 0.04 \pm 0.02$  and has a staggered crystal structure. The staggered crystal structure would cause the staggered  $g$  tensor, which produces an effective staggered field when an external magnetic field is applied. Thus it would be interesting to measure ESR in  $\text{MnCl}_3(\text{bpy})$  and compare to the present theory.

Our results may be applied to a wider range of one-dimensional systems such as quantum spin ladders as well, since they can also be described by the same CRM<sup>6</sup>. For spin ladders, there are various possible generalizations of the staggered field. The results of the present paper can be directly applied when the staggered field is unfrustrated<sup>18,19</sup>, for example as in

$$\begin{aligned} \mathcal{H} = & \sum_{\mu=1}^n \sum_j [J \mathbf{S}_{\mu,j} \cdot \mathbf{S}_{\mu,j+1} - HS_{\mu,j}^z - (-1)^{\mu+j} h S_{\mu,j}^x] \\ & + \sum_{\mu=1}^{n-1} \sum_j J_{\perp} \mathbf{S}_{\mu,j} \cdot \mathbf{S}_{\mu+1,j}, \end{aligned} \quad (8)$$

where  $n$  is the number of legs and  $\mu$  is the leg index. In this case, the staggered field can be handled in the same way as in the chain (7).

In fact, even for gapless one-dimensional systems such as half-integer spin Heisenberg antiferromagnetic chains,  $\Delta$  defined in Eq. (5) is a characteristic energy scale. At energy scales of order  $\Delta$ , the system renormalizes from the weak coupling regime, where classical methods can be used, to the non-trivial critical point induced by the topological term in the effective Lagrangian. At temperatures small compared to  $\Delta$  the low temperature theory for the  $S = 1/2$  Heisenberg model<sup>15,16</sup> can be used. (For the  $S = 1/2$  case, this theory is valid at any tempera-

ture  $T \ll J$ .) On the other hand, in the temperature range (6), the present approach based on the CRM is valid even in gapless systems.

Physically, ESR in the presence of the staggered field provides an interesting case of crossover of dynamics between two different regimes. When the effect of the staggered field is weak, the ESR spectrum is dominated by the paramagnetic resonance at  $\omega \sim H$ , and the staggered field causes its broadening and shift. However, when the effect of the staggered field is strong, the system is ordered along the staggered field. The ESR spectrum is dominated by the spin-wave type fluctuation around the ordered state. This is similar to the case in which the system has a Néel order spontaneously, but is different in that the “order” is imposed externally by the staggered field. Nevertheless, theory of antiferromagnetic resonance<sup>20,21</sup> developed for the spontaneously ordered state can be modified and applied to the present case, as discussed for example in Ref. 10. It describes the limit of the strong staggered field, where the imposed Néel order is perfect.

In the case of a spontaneous ordering, a phase transition separates the ordered and disordered phases. In the present case, there is no phase transition but only a smooth crossover between the two regimes. The description of the crossover is generally much more difficult than that of the limiting cases.

For the  $S = 1/2$  chain, the field theory approach successfully gives the broadening and shift of the paramagnetic resonance, when the staggered field is small (or the temperature is sufficiently high). It also explains the ESR spectrum in the low temperature limit, when the system is ordered along the staggered field. The antiferromagnetic resonance in this case is renormalized due to strong quantum fluctuations in the  $S = 1/2$  chain. This can be well described in terms of elementary excitations of quantum sine-Gordon field theory. However, despite the integrability of the quantum sine-Gordon field theory, dynamical susceptibility at finite temperature has not been obtained exactly. Thus the theoretical description of the crossover between two regimes still remains unsolved, although a numerical result based on exact diagonalization was reported<sup>22</sup>.

In other systems, the crossover is even less understood. The present approach can, where it is valid, numerically describe the nontrivial crossover of the ESR spectrum between two regimes as we will demonstrate.

This paper is organized as follows. In Sec. II, we introduce the quantum O(3) NLSM as an effective low-energy theory for the Hamiltonian (7), and review its renormalization. ESR spectrum is also formulated in terms of the O(3) NLSM. We will then discuss the classical approximation of the O(3) NLSM, including the range of validity of the approximation, in Sec. III. The CRM is introduced as a lattice version, suitable for numerical calculation, of the classical limit of the O(3) NLSM. In Sec. IV we will obtain ESR spectra by numerically solving the equation of motion for the CRM. We will develop a theory of anti-

ferromagnetic spin-wave resonance in Sec. V, which can be identified with the new resonance at higher frequency found in the numerical results. Finally in Sec. VI we summarize the paper.

## II. O(3) NONLINEAR SIGMA MODEL

### A. Definition of the model

Let us introduce the O(3) NLSM as an effective field theory of the antiferromagnetic Heisenberg chain, and summarize its properties. Although we will eventually treat the system classically, first we need to clarify the effects of quantum fluctuation in order to determine the appropriate parameters in the effective classical model.

The O(3) NLSM is defined in terms of two fields  $\mathbf{n}(x)$  and  $\mathbf{L}(x)$  which are related to the original spin  $\mathbf{S}_j$  through

$$\mathbf{S}_j = (-1)^j S \mathbf{n}(x) \sqrt{1 - \left(\frac{a\mathbf{L}(x)}{S}\right)^2} + a\mathbf{L}(x). \quad (9)$$

Here  $x = ja$ , and  $a$  is a lattice spacing. Hereafter we set the lattice spacing to  $a = 1$ .  $\mathbf{n}(x)$  and  $\mathbf{L}(x)$  satisfy constraints

$$\mathbf{n}^2(x) = 1, \quad (10)$$

$$\mathbf{n}(x) \cdot \mathbf{L}(x) = 0, \quad (11)$$

which are necessary to keep the constraint  $\vec{S}^2 = S(S+1)$ . Then  $\mathbf{n}(x)$  and  $\mathbf{L}(x)$  satisfy the following commutation relations

$$[L^\alpha(x), L^\beta(y)] = i\epsilon^{\alpha\beta\gamma} L^\gamma(x) \delta(x-y), \quad (12)$$

$$[L^\alpha(x), n^\beta(y)] = i\epsilon^{\alpha\beta\gamma} n^\gamma(x) \delta(x-y), \quad (13)$$

$$[n^\alpha(x), n^\beta(y)] = 0. \quad (14)$$

O(3) NLSM is derived after substituting (9) to (7) and taking the continuum limit. The Hamiltonian density of O(3) NLSM is given by

$$\mathcal{H} = \frac{c}{2g} (\partial_x \mathbf{n})^2 + \frac{cg}{2} \mathbf{L}^2 - HL^z - \frac{\Delta_h^2}{gc} n^x, \quad (15)$$

where  $c = 2JS$  is the spin-wave velocity,  $g = 2/S$  is the coupling constant, and  $\Delta_h$  is defined as

$$\Delta_h = \sqrt{4JS\hbar}, \quad (16)$$

Later in this Section, we will show that  $\Delta_h$  is the staggered-field-induced gap. The coupling constant  $g$  is actually subject to renormalization owing to quantum fluctuations, which we will discuss in the next subsection.  $g = 2/S$  should be understood as the bare coupling constant.

Here we introduce useful normalization which measure the energy scale in units of  $c = 2JS$ .

$$\mathcal{H}' = \frac{\mathcal{H}}{2JS} \quad (17a)$$

$$T' = \frac{T}{2JS} \quad (17b)$$

$$H' = \frac{H}{2JS} \quad (17c)$$

$$h' = \frac{h}{2JS} \quad (17d)$$

$$\Delta'_h = \frac{\Delta_h}{2JS} = \sqrt{2h'} \quad (17e)$$

$$t' = 2JS t \quad (17f)$$

$$\omega' = \frac{\omega}{2JS} \quad (17g)$$

We specify the normalized, dimensionless parameters by adding the prime symbol as in the above. In this notation, the Hamiltonian (15) is rewritten as

$$\mathcal{H}' = \frac{1}{2g}(\partial_x \mathbf{n})^2 + \frac{g}{2}\mathbf{L}^2 - H' L^z - \frac{\Delta_h'^2}{g} n^x. \quad (18)$$

Because Eq. (15) (or Eq. (18)) is harmonic in  $\mathbf{L}(x)$ ,  $\mathbf{L}(x) - \mathbf{H}/gc = \mathbf{n} \times (\partial_t \mathbf{n} + \mathbf{H} \times \mathbf{n})/gc = \mathbf{n} \times (\partial_t \mathbf{n} + \mathbf{H}' \times \mathbf{n})/g$  can be integrated out. Then the Lagrangian is given by

$$\begin{aligned} \mathcal{L}' &= \partial_t \mathbf{n} \cdot (\partial_t \mathbf{n} + \mathbf{H}' \times \mathbf{n}) - \mathcal{H}' \\ &= \frac{1}{2g}(\partial_t \mathbf{n} + \mathbf{H}' \times \mathbf{n})^2 - \frac{1}{2g}(\partial_x \mathbf{n})^2 + \frac{\Delta_h'^2}{2g} n^x, \end{aligned} \quad (19)$$

with the constraint (10). In this expression, it is clear that the coupling constant  $g$  represents the degree of quantum fluctuation, since it plays the role of Planck's constant.

Although there is no energy scale in the Lagrangian density, O(3) NLSM at  $H = h = 0$  has an excitation gap, which corresponds to the Haldane gap  $\Delta$ . In field theory language, the mass gap is dynamically generated. The low-energy phenomena of the O(3) NLSM can be effectively described by the field theory of triplet bosons with the mass  $\Delta$ :

$$\mathcal{L} = \frac{c}{2g}(\partial_\mu \mathbf{n})^2 - \frac{1}{2gc}\Delta^2 \mathbf{n}^2(x), \quad (20)$$

without the constraint (10). Hereafter  $(\partial_\mu \mathbf{n})^2$  means  $(\partial_\mu \mathbf{n})^2 = (1/c^2)(\partial_t \mathbf{n})^2 - (\partial_x \mathbf{n})^2 = (\partial_t \mathbf{n})^2 - (\partial_x \mathbf{n})^2$ .

When the applied field  $H$  becomes larger than  $\Delta$  while the staggered field  $h = 0$ , the gap is closed. On the other hand, when staggered field  $h$  is large, the excitation gap is still open even if  $H > \Delta$  because the Lagrangian (19) is approximated as follows.

$$\mathcal{L}' = \frac{1}{2g}(\partial_\mu \mathbf{m})^2 - \frac{\Delta_y'^2}{2g}(m^y)^2 - \frac{\Delta_z'^2}{2g}(m^z)^2, \quad (21)$$

where  $\Delta'_\alpha = \sqrt{H'^2 \delta_{\alpha,z} + \Delta_h'^2}$ . The field  $\mathbf{m} = (0, n^y, n^z)$  contains the components of  $\mathbf{n}$  transverse to the staggered field direction. We assumed  $n^x(t, x) \approx 1$  because of large  $h$ .  $\mathbf{m}$  represents the elementary excitation in the large  $h$  regime and has a dispersion  $E_k^{(\alpha)} = \sqrt{k^2 + \Delta'_\alpha{}^2}$  where  $k$  is the wave number and  $\alpha = y, z$ . This dispersion relation indicates that the gap for the  $z$  component is different from the gap for the  $y$  component:

$$\Delta'_z = \sqrt{H'^2 + \Delta_h'^2}, \quad (22)$$

$$\Delta'_y = \Delta'_h, \quad (23)$$

where  $\Delta'_h$  is the staggered-field-induced gap (17e). The gap (22) is derived within the classical approximation ignoring quantum fluctuation. On the other hand, in the absence of the staggered field, the quantum fluctuation leads to the Haldane gap  $\Delta$ . Roughly speaking, the excitation gap of the system is given as

$$\tilde{\Delta}' \sim \max(\Delta', \Delta'_h) \quad (24)$$

In ESR measurements, we apply an oscillating field with frequency  $\omega$  and polarization  $\alpha$ . In this paper we consider Faraday configuration where the polarization is perpendicular to the direction of the uniform field. ESR absorption intensity

$$I(\omega) \propto \omega \chi''_{\alpha\alpha}(\omega), \quad (25)$$

is written in terms of the dynamical susceptibility  $\chi_{\alpha\alpha}(\omega)$ . According to the linear response theory, the imaginary part of  $\chi_{\alpha\alpha}(\omega)$  is related to Fourier component of the retarded Green function  $G_{\alpha\alpha}^R(t) = -i\theta(t)\langle [L_T^\alpha(t), L_T^\alpha(0)] \rangle$ , namely  $\chi''_{\alpha\alpha}(\omega) = -\text{Im} G_{\alpha\alpha}^R(\omega)$ . The retarded Green function  $G_{\alpha\alpha}^R(\omega)$  is defined as

$$G_{\alpha\alpha}^R(\omega) = -i \int_0^\infty dt e^{i\omega t} \langle [L_T^\alpha(t), L_T^\alpha(0)] \rangle. \quad (26)$$

$L_T^\alpha = \int dx L^\alpha(x)$  is the total magnetization. In general, the ESR spectrum thus depends on the polarization  $\alpha$ .

In Ref. 16, it was shown that for the system (7) with the staggered field in  $x$ -direction, the polarization dependence can be exactly determined by the equation of motion:

$$\chi''_{\alpha\alpha}(\omega) = \frac{H^2 \cos^2 \Phi + \omega^2 \sin^2 \Phi}{\omega^2} \chi''_{yy}(\omega), \quad (27)$$

where  $\Phi$  is the angle between the polarization  $\alpha$  and  $x$ -axis.

Furthermore, ESR spectrum for circular polarization can be related to

$$\chi''_{+-}(\omega) = \text{Re} \int_0^\infty dt e^{i\omega t} \langle [L_T^+(t), L_T^-(0)] \rangle, \quad (28)$$

where  $L^\pm = L^x \pm iL^y$ . The discussion in Ref. 16 can be extended to circular polarization to obtain

$$\chi''_{+-}(\omega) = \left(1 + \frac{H}{\omega}\right)^2 \chi''_{yy}(\omega). \quad (29)$$

That is, ESR spectra for different polarization in Faraday configuration are related to each other, and thus it is sufficient to compute the spectrum for one particular case.

In this paper, we consider the circular polarization case, eq. (28). A short calculation yields

$$\chi''_{+-}(\omega) = (1 - e^{-\omega/T}) \operatorname{Re} \int_0^\infty dt e^{i\omega t} \langle L_T^+(t) L_T^-(0) \rangle, \quad (30)$$

which is convenient for our purpose since eq. (30) is well-defined even if  $L^\alpha(t)$  is a classical vector. In this paper, we numerically solve the classical equation of motion to obtain the dynamical correlation function

$$\langle L_T^+(t) L_T^-(0) \rangle. \quad (31)$$

This gives the desired ESR spectrum by eq. (30). Our numerical approach to this problem will be discussed in Sec. III and Appendix B.

### B. Renormalization group transformation

Let us consider the renormalization group transformation of general  $O(N)$  NLSM whose Lagrangian is given by

$$\mathcal{L}' = \frac{1}{2g} (\partial_t \mathbf{n} + \mathbf{H}' \times \mathbf{n})^2 - \frac{1}{2g} (\partial_x \mathbf{n})^2 + \frac{2h'}{g} n^x. \quad (32)$$

This bare theory is defined at the energy scale  $J$ . we renormalize this theory down to an energy scale  $E < J$ .

When  $H = h = 0$ , the effective coupling  $g_R(E)$  at energy scale  $E$  satisfies<sup>23</sup>

$$\frac{1}{g} - \frac{1}{g_R(E)} = \frac{N-2}{2\pi} \ln \left( \frac{E}{J} \right). \quad (33)$$

As the bare coupling satisfies  $1/g = (N-2) \ln(J/\Delta)/2\pi$ , we can simplify the renormalized coupling constant

$$\frac{1}{g_R(E)} = \frac{N-2}{2\pi} \ln \frac{E}{\Delta}. \quad (34)$$

For the case of our interest,  $N = 3$ , we find

$$g_R(E) = \frac{2\pi}{\ln(E/\Delta)}. \quad (35)$$

Next we consider the renormalization of the staggered field. We ignore the influence of  $h'$  on the renormalization of  $g$ , but consider the renormalization of  $h'$  produced by  $g$ , at lowest order. This is determined by the anomalous dimension of the field  $\mathbf{n}$ <sup>23,24</sup>.

$$\frac{\partial h'_R}{\partial \ln E} = -\gamma(g_R(E)) h'_R \quad (36)$$

To one loop order, the anomalous dimension  $\gamma(g)$  is

$$\gamma(g) = -\frac{N-3}{4\pi} g \quad (37)$$

Using Eq. (33) for  $g_R(E)$ , Eq. (36) becomes:

$$\frac{d \ln h'_R}{d \ln E} = -\frac{N-3}{2(N-2)} \frac{1}{\ln(E/\Delta)} \quad (38)$$

This gives the renormalized staggered field

$$h'_R(E) = h' \left[ \frac{\ln(E/\Delta)}{\ln(J/\Delta)} \right]^{(N-3)/2(N-2)}. \quad (39)$$

Namely, for the case of our interest  $N = 3$ , the renormalization of the staggered field  $h'$  is absent. The renormalized Lagrangian is given by just replacing  $g$  by  $g_R(E)$  in eq. (19). Because  $h'_R(E) = h'$  is kept unchanged (within the leading order considered in this paper) for  $N = 3$ , there is no logarithmic correction in the staggered-field-induced gap (16)

## III. CLASSICAL APPROXIMATION

### A. Conditions for the classical approximation

In the Introduction, we have briefly discussed the condition (6) for the classical approximation being justified. Here we discuss the condition in some more detail, with several additional conditions.

The latter condition in eq. (6),

$$T \ll JS^2, \quad (40)$$

is required for the validity of the effective theory in the continuum. It is equivalent to the requirement that the correlation length of the antiferromagnetic order parameter is much longer than the lattice spacing. In fact, as pointed out in Ref. 6, two different temperature regimes can be distinguished for large  $S$ .

$$T < T_{\max}^{(1)} \sim 2JS, \quad (41)$$

and

$$T_{\max}^{(1)} \sim 2JS < T < T_{\max}^{(2)} \sim JS^2. \quad (42)$$

In the regime (41), the  $O(3)$  NLSM description is valid. On the other hand, when eq. (42) holds, the quantum spin chain may be directly approximated as a classical spin chain and then the continuum description is applied. The resulting dynamics is equivalent to that of the classical  $O(3)$  NLSM, although the effective parameters are estimated in a different manner. For simplicity, throughout the rest of this paper, we assume the regime (41). Although ESR in the higher temperature range  $T_{\max}^{(2)} \sim JS^2 \lesssim T$  is also an interesting nontrivial problem, it is out of scope of the present paper.

ESR is studied under an applied magnetic field  $H$ . If the ground state is fully polarized along  $H$ ,  $O(3)$  NLSM is not appropriate as an effective theory. Thus, our approach also requires that the uniform field should be

much weaker than its saturation field, which is order of  $JS$ :

$$H \ll JS. \quad (43)$$

The first inequality in eq. (6) is necessary for the classical approximation to hold. Namely, that the temperature higher than the gap, implies high density of thermally excited magnons. This leads to a breakdown of the quantum mechanical picture<sup>7</sup> of ESR based on transitions of independent magnons. In fact, as we have discussed in Sec. II A, the staggered field induces a gap as in eq. (16). Since actual gap of the system is given as eq. (24), the first inequality in eq. (6) should be replaced by

$$\tilde{\Delta} = \max(\Delta, \Delta_h) \ll T. \quad (44)$$

Namely, the temperature must be higher than not only the Haldane gap  $\Delta$ , but also the staggered-field induced gap  $\Delta_h$ . Together with eqs. (40) and (16), this requires

$$h \ll \frac{T^2}{4JS} \ll \frac{JS^3}{4}. \quad (45)$$

Later, we will discuss an antiferromagnetic spin-wave theory of ESR. It is justified when

$$h \gg \frac{\pi^2 T^2}{4JS(\ln(T/\Delta))^2}, \quad (46)$$

where we have assumed eq. (48). For a larger spin  $S$ , the Haldane gap  $\Delta$  is expected to become exponentially small as in eq. (5). Thus the range of  $h$  satisfying both eqs. (45) and (46) becomes wide for large  $S$ . In fact, we will demonstrate that the spin-wave theory prediction agrees very well for a  $S = 10$  chain with staggered field, in a range of parameters. On the other hand, for  $S = 2$ , when the classical approximation is valid, the spin-wave theory is not quite justified. Correspondingly, a broad peak is observed instead of a sharp resonance. Nevertheless, the broad peak may be understood as a remnant of the spin-wave resonance.

For discussion of ESR based on the classical dynamics of the NLSM, the frequency  $\omega$  of the applied oscillating field also should be much lower than the temperature.

$$\omega \ll T \quad (47)$$

This also implies

$$H \ll T, \quad (48)$$

because ESR absorption usually occurs for  $\omega \geq H$ .

## B. Effective Hamiltonian

In the Introduction, we argued that the system should be described by the classical O(3) NLSM in the intermediate temperature range (6).

Even in the temperature range (6), we cannot simply ignore quantum fluctuations at energy scale above the temperature  $T$ . Their effects are taken into account by the renormalization group. The effective classical Hamiltonian for the O(3) NLSM may be obtained by using the renormalized parameters, eqs. (35) and (39), and setting the energy scale to the temperature:  $E = T$ .

On the other hand, we do not consider the renormalization of  $\mathbf{H} \cdot \mathbf{L}$  term since  $\int dx \mathbf{L}$  is a conserved quantity when  $h = 0$ . Therefore any renormalization that does occur should vanish at  $h = 0$  and would be negligible at small  $h$ . The renormalized Hamiltonian density is thus given as

$$\mathcal{H}_{\text{cl}} = \frac{c}{2g_R} (\partial_x \mathbf{n})^2 + \frac{cg_R}{2} \mathbf{L}^2 - HL^z - \frac{\Delta_h^2}{2cg_R} n^x, \quad (49)$$

where  $g_R = g_R(T)$ . In terms of dimensionless parameters, it reads

$$\mathcal{H}'_{\text{cl}} = \frac{1}{2g_R} (\partial_x \mathbf{n})^2 + \frac{g_R}{2} \mathbf{L}^2 - H' L^z - \frac{2h'}{g_R} n^x. \quad (50)$$

As we will discuss below, the coefficient of the  $(\partial_x \mathbf{n})^2$  term and the  $\mathbf{L}^2$  term in the classical Hamiltonian (49) can be identified respectively with  $\xi T/2$  and  $1/2\chi_{u\perp}$ , where  $\xi$  is the classical correlation length of  $\mathbf{n}$  and  $\chi_{u\perp} = (3/2)\chi_u$  is proportional to the zero-field uniform susceptibility  $\chi_u$ , both at zero fields  $H = h = 0$ . Namely,

$$\xi = \frac{c}{2\pi T} \ln \frac{T}{\Delta} \quad (51)$$

$$\chi_{u\perp} = \frac{1}{2\pi c} \ln \frac{T}{\Delta} \quad (52)$$

Thus, the effective Hamiltonian density (49) can be also written as

$$\mathcal{H}_{\text{cl}} = \frac{\xi T}{2} (\partial_x \mathbf{n})^2 + \frac{1}{2\chi_{u\perp}} \mathbf{L}^2(x) - HL^z(x) - \chi_{u\perp} \Delta_h^2 n^x, \quad (53)$$

which is the form used in Ref. 6.

In numerical calculations we discretize the effective field theory (50) and consider the Hamiltonian,

$$\mathcal{H}'_{\text{cl}} = \sum_j b \left[ -\frac{1}{b^2 g_R} \mathbf{n}_j \cdot \mathbf{n}_{j+1} + \frac{g_R}{2} \mathbf{L}_j^2 - H' L_j^z - \frac{2h'}{g_R} \Delta_h^2 n^x \right], \quad (54)$$

on a lattice with the lattice spacing  $b$ . This is nothing but the CRM (1) in dimension  $D = 1$ . We note that it is not necessary to take  $b$  equal to the lattice spacing  $a = 1$  of the original spin chain; the CRM may be regarded as a lattice regularization of the classical, continuum O(3) NLSM. Usually  $b \geq a$  is taken, because the eq. (54) is introduced to describe long-distance asymptotic behavior of the spin system. The system size  $L = \mathcal{N}b$  is proportional to the number of rotors  $\mathcal{N}$ . We use  $\mathcal{N} = 16$  for our numerical calculations. As we will see in FIG. 1,  $\mathcal{N} = 16$  is large enough to reproduce consistent values

of the magnetization density  $M/L$  with quantum Monte Carlo calculations and low-field expansion. This is because the correlation length of  $\mathbf{n}_j$  is much shorter than  $L$  due to the relatively high temperature  $T \sim J$ .

Let us now demonstrate that the above identifications are valid within the classical theory. To do so, we assume the Hamiltonian density in the form of eq. (53), and then show that  $\xi$  and  $\chi_u$  are indeed the correlation length and the uniform susceptibility. To calculate the correlation function of  $\mathbf{n}$ , it is convenient to integrate out  $\mathbf{L}$  and obtain the Hamiltonian in terms of  $\mathbf{n}$ . For  $H = h = \Delta_h = 0$ , it reads

$$\mathcal{H}_{\text{eff}} = \frac{T\xi}{2} \int dx \left( \frac{d\mathbf{n}}{dx} \right)^2 \approx -\frac{T\xi}{b} \sum_j \mathbf{n}_j \cdot \mathbf{n}_{j+1}. \quad (55)$$

The last expression is the NLSM Hamiltonian on a discretized one-dimensional lattice with the lattice constant  $a$ . In fact, it is equivalent to the classical Heisenberg chain. The equilibrium statistical properties of the classical Heisenberg chain are studied by Fisher<sup>25</sup>. The correlation function  $\langle n^a(x)n^b(0) \rangle$  of the classical Hamiltonian (55) is obtained exactly by using transfer matrix method,  $\langle n^a(x)n^b(0) \rangle = (1/3)\delta^{ab} \exp(-|x|/\xi)$ , which indicates that Eq. (51) is indeed the correlation length of the order parameter  $\mathbf{n}$ .

Next we introduce an infinitesimal uniform field  $\mathbf{H}$ . The zero-field uniform susceptibility  $\chi_u$  is defined as  $\chi_u = \lim_{H \rightarrow 0} dM/dH$  where  $M = \int dx \langle L^z \rangle$  is the total magnetization. We calculate the uniform susceptibility  $\chi_u$  of the classical NLSM (53), with  $h = \Delta_h = 0$ . After integrating out  $\mathbf{L}$ , the Hamiltonian becomes

$$\mathcal{H} = \int dx \left[ \frac{T\xi}{2} \left( \frac{d\mathbf{n}}{dx} \right)^2 - \frac{\chi_{u\perp} H^2}{2} (\mathbf{n}^\perp)^2 \right]. \quad (56)$$

Here we defined  $\mathbf{n}^\perp = (n^x, n^y, 0)$ . The uniform susceptibility is thus obtained as

$$\chi_u = \lim_{H \rightarrow 0} \chi_{u\perp} \int dx \langle (\mathbf{n}^\perp)^2 \rangle = \frac{2}{3} \chi_{u\perp}, \quad (57)$$

where  $\langle \cdot \rangle$  is the thermodynamic expectation value at  $H = 0$ .  $\langle (\mathbf{n}^\perp)^2 \rangle = 2/3$  follows from the isotropy of the Hamiltonian and the constraint (10). Thus, (52) is proved to be a transverse component of the uniform susceptibility  $\chi_u$ .

### C. Magnetization

Our primary interest in this paper is in the dynamics of the system. However, before going into the dynamics, it would be important to establish the validity of the present approach by considering static properties. This was done earlier in Ref. 26, in the zero field limit.

Here we demonstrate its validity for nonzero magnetic field  $H$ , which is relevant for ESR, by discussing the magnetization and its dependence on  $H$  and  $T$ . In a classical

system with U(1) symmetry around  $H$  (thus with  $h = 0$ ), we find the following interesting identity

$$M = \frac{H}{T} \int dx dy \langle L^x(x)L^x(y) \rangle_{\text{cl}}, \quad (58)$$

where  $M = \langle L_T^z \rangle_{\text{cl}}$  is the classical uniform magnetization. This identity is valid for any  $H$  and  $T$ . The proof of (58) is given in the Appendix A. We can easily confirm that this classical magnetization is approximately equal to the uniform magnetization of the corresponding quantum chain.

Since we approximate the renormalization group equation at the lowest order, the uniform field  $\mathbf{H}$  and the staggered field  $\mathbf{h}$  do not affect the renormalization of the coupling constant  $g$ , except that  $H$  gives the energy scale  $E$  for the renormalization if  $H > T$ . At small but finite field, the uniform susceptibility has a small deviation from (57), which is proportional to  $H^2$ . We expand the uniform magnetization  $M$  with respect to small  $H$ :

$$\frac{M}{L} \approx \chi_{u\perp} H \left[ \frac{2}{3} + \frac{\chi_{u\perp} H^2}{2} \int dx \langle (\mathbf{n}^\perp(x))^2 (\mathbf{n}^\perp(0))^2 \rangle_0 \right]$$

$\langle \cdot \rangle_0$  denotes the thermal average by the classical zero-field Hamiltonian (56). The second term can be calculated by using the following formula for four-point function,

$$\begin{aligned} & \langle n^a(x)n^b(x)n^c(0)n^d(0) \rangle_{\text{cl}} \\ &= \frac{1}{9} \delta^{ab} \delta^{cd} + \frac{e^{-3|x|/\xi}}{45} (3(\delta^{ac} \delta^{bd} + \delta^{ad} \delta^{bc}) - 2\delta^{ab} \delta^{cd}), \end{aligned}$$

and the result is,

$$\frac{M}{L} = \chi_{u\perp} H \left[ \frac{2}{3} + \frac{4}{135} \frac{\xi \chi_{u\perp} H^2}{T} \right] + O(H^5). \quad (59)$$

The uniform (differential) susceptibility is given by

$$\begin{aligned} \chi_u &= \frac{2}{3} \chi_{u\perp} \left[ 1 + \frac{2}{15} \frac{\chi_{u\perp} \xi H^2}{T} \right] \\ &= \frac{1}{3\pi c} \ln \left( \frac{\max(T, H)}{\Delta} \right) \left[ 1 + \frac{cH^2}{15\pi T^2} \ln^2 \left( \frac{\max(T, H)}{\Delta} \right) \right]. \end{aligned} \quad (60)$$

We employ the energy scale  $E = \max(T, H)$  in the log correction in (59) and (61) instead of  $E = T$  as in the previous Section, because the magnetic field can exceed the temperature when we do not consider ESR. If  $H > T$ , we should take a cut-off scale as  $E = H$ .

We have calculated the magnetization density in the quantum  $S = 2$  antiferromagnetic chain by quantum Monte Carlo simulation, and also in the effective CRM by classical Monte Carlo (CMC) simulation. Our method of CMC simulations of the O(3) CRM is explained in Appendix B. The quantum Monte Carlo simulation was done using the codes provided by ALPS project<sup>27,28</sup>. In the  $S = 2$  chain, the magnetization density is defined simply by  $M/L = \langle S_T^z \rangle / L$ . The numerical results are compared with the low-field expansion (59) in Fig. 1.

The magnetization density in the quantum  $S = 2$  chain agrees well with that in the effective classical  $O(3)$  NLSM, and with eq. (59). We note that there is no adjustable parameter in this comparison, owing to the fact that the magnetization is a conserved quantity. For higher field  $H$ , there is a visible discrepancy between the numerical results and the analytical prediction (59). This is presumably due to the higher order terms in  $H$  which are ignored in eq. (59), and not because of breakdown of the classical description. In fact, the CMC result for the effective classical  $O(3)$  NLSM agrees quite well with the quantum  $S = 2$  chain, even at higher field  $H$ .

In Fig. 2 we show the difference between the magnetization density calculated by the CMC simulations and the low field expansion (59). The difference between the two results is indeed proportional to  $H^5$ , which is the next order in the expansion. These results on the magnetization supports the validity of the classical description for  $S \geq 2$  chain, also in a finite magnetic field  $H$ .

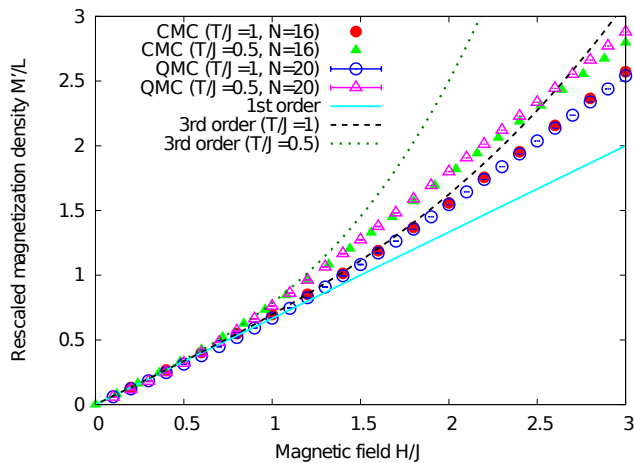


FIG. 1. The rescaled magnetization density  $M'/L = M/L \times 1/(J\chi_{u\perp})$  for  $O(3)$  NLSM is plotted. The open circles and triangles are numerical data by classical Monte Carlo simulation. The filled circles and triangles with error bars are obtained by quantum Monte Carlo simulation. We found finite-site effects in QMC data very small, by comparing simulations on 20 sites and 40 sites. We set the unit of the vertical axis so that the simple relation  $M'/L \approx (2/3)H'$  holds at low  $H' \equiv H/J < 1$ . The solid line represents the low field expansion of  $M/L$  up to 1st order of  $H$ , which is  $M'/L = M/(LJ\chi_{u\perp}) = \frac{2}{3}(H/J)$  by (59). The dashed and dotted lines are 3rd order approximations of (59) at temperature  $T/J = 1$  and  $T/J = 0.5$  respectively. The low  $H$  expansion (59) is consistent with the numerical data in the regime  $H/T \lesssim 1$ . We emphasize that CMC and QMC data are consistent in any value of the magnetic field.

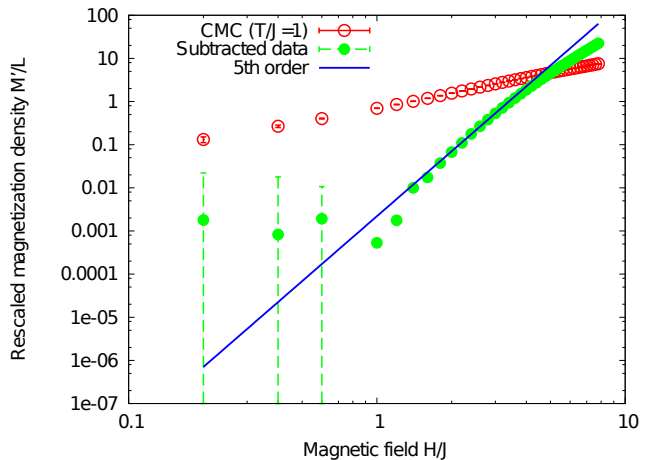


FIG. 2. The open circles are the classical Monte Carlo data ( $T/J = 1$ ) which are shown in Fig. 1. The filled circles are the difference of CMC data and (59). This subtracted data agree well with the solid line  $0.0022 \times H^5$  whose coefficient is determined by fitting.

#### D. Equations of motion

The classical dynamics of the CRM (54) is studied by solving the classical equation of motion. In the classical theory, the commutation relations (12), (13) and (14) are replaced by the Poisson brackets (4). These brackets lead to the equations of motion,

$$\frac{d\mathbf{n}_j}{dt'} = (g_R(T)\mathbf{L}_j - \mathbf{H}') \times \mathbf{n}_j, \quad (62)$$

$$\frac{d\mathbf{L}_j}{dt'} = \frac{1}{g_R(T)b^2} \mathbf{n}_j \times (\mathbf{n}_{j+1} + \mathbf{n}_{j-1}) - \mathbf{H}' \times \mathbf{L}_j - \frac{\Delta_h'^2}{g_R(T)} \mathbf{e}_x \times \mathbf{n}_j. \quad (63)$$

#### IV. ESR SPECTRUM

In the present approach, the ESR spectrum is obtained from the classical dynamics of the effective  $O(3)$  NLSM theory. The classical dynamical correlation function is calculated as follows. First we generate initial states using the classical Monte Carlo Method so that the probability distribution of initial states is identical to the Boltzmann weight with the Hamiltonian (53) at given temperature. For each initial state, we solve the equations of motion (62) and (63) numerically. We must pay careful attention to the total energy, which is a conserved quantity. Determination of the ESR lineshape requires the asymptotic, long-time behavior of the dynamical correlation function. The time evolution was obtained up to time  $t'_{\max} = 2000$  with the time step  $\delta t' = 0.001$ .

Naïve numerical integration of the equations of motion results in violation of the energy conservation. This makes the scheme unsuitable for ESR calculation, for

which, as we have discussed in the Introduction, high accuracy is required. We applied symplectic methods<sup>29,30</sup> to assure the conservation law. We will give detailed explanations about these numerical methods in Appendix B. The initial state is generated by classical Monte Carlo simulation of the O(3) NLSM at the given temperature.

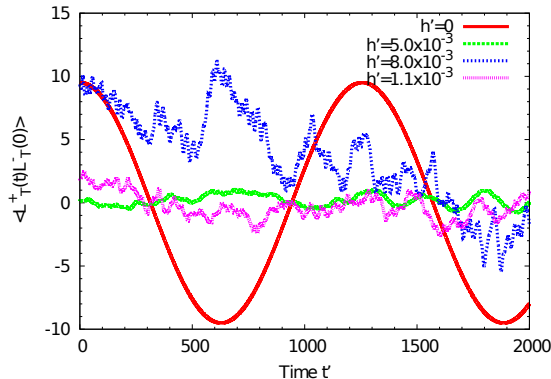


FIG. 3. Time evolution of  $L_T^+(t)L_T^-(0)$  for  $S = 2$ ,  $T' = 0.15$ , and  $H' = 0.005$ , obtained by solving classical equation of motion for one initial state generated by the classical Monte Carlo simulation. The time evolution appears chaotic for nonzero staggered field  $h'$ , before taking ensemble average.

An example of the time evolution of  $L_T^+(t)L_T^-(0)$  obtained by numerically solving the equation of motion, for one initial state is shown in Fig. 3. For zero staggered field, its exact solution is given by harmonic oscillation. However, in the presence of a nonvanishing staggered field, the time evolution looks chaotic. After Fourier transform, the spectrum is also noisy reflecting the “noise” in the time evolution.

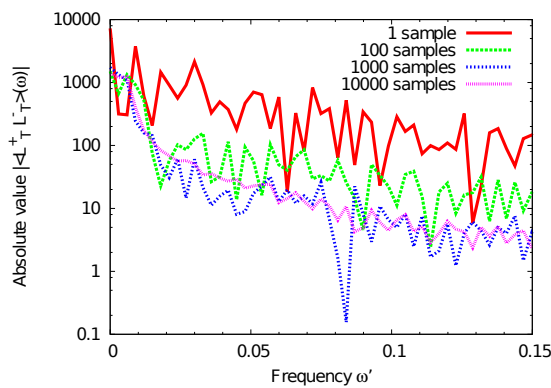


FIG. 4. The Fourier transform  $|\langle L_T^+ L_T^- \rangle|(\omega')$  of the dynamical correlation function (31) for  $S = 2$ ,  $T' = 0.15$ ,  $H' = 0.005$ , and  $h' = 0.008$ , obtained by averaging over various number of sample initial states. The approximately white noise is reduced by increasing the number of samples.

The correlation function (31) is defined by thermal ensemble average over initial states. In our calculation, the above steps are repeated for  $10^4$  Monte Carlo samples of initial states, and the average is taken. After taking the average, we obtain the dynamical correlation  $\langle L_T^+(t)L_T^-(0) \rangle$ . The averaging over many samples of the initial states reduces the noise in the spectrum. In Fig. 4 we show the absolute value of the dynamical correlation function (31) at  $h' = 0.008$ , obtained by average over 1, 100, 1000, and 10000 samples of initial states. We note that the data contains both signal and noise. For 10000 samples, the result shows small fluctuation due to noise, around the signal. For 1 sample, on the other hand, the observed data is dominated by the noise, which randomly takes positive or negative values. (In Fig. 4, the absolute value is shown.)

In the range of frequency  $0 < \omega' < 0.15$  we are interested, the power spectrum of the noise is approximately independent of the frequency  $\omega'$ ; it may be regarded as a white noise. The reduction of the noise by averaging is clear in the figure, and the noise is proportional to  $1/\sqrt{N_s}$ , where  $N_s$  is the number of initial state samples. However, for a realistic number of samples (we used  $N_s \sim 10^4$ ) the noise is still not completely negligible. This effectively constrains resolution in the frequency, as we discuss below.

Because of the finite time interval  $t'_{\max}$ , resolution in the frequency space is at most  $2\pi/t'_{\max} \sim 0.003$ . It is well known that a simple Fourier transform of the time dependence up to the cutoff time  $t'_{\max}$  leads to an artificial spreading of resonances known as spectral leakage.<sup>31</sup> To suppress the spectral leakage, a window function is multiplied to the data before Fourier transform. Here we apply the Gauss window function.<sup>32,33</sup> Namely, instead of  $\langle L_T^+(t)L_T^-(0) \rangle$ , we take the Fourier transformation of

$$\langle L_T^+(t)L_T^-(0) \rangle \exp\left(-\frac{t^2}{2\sigma^2}\right). \quad (64)$$

Obviously, the width of the Gaussian window  $\sigma$  must be smaller than  $t'_{\max}$ . Usually the width  $\sigma$  is still taken as the same order as  $t'_{\max}$ , for example  $\sigma \sim 0.4t'_{\max}$ . However, we find that the obtained spectrum is affected by the noise for such a choice of  $\sigma$ . In order to reduce the noise, we take  $\sigma$  much smaller than  $t'_{\max}$ . The reduction of the noise by windowing is discussed in Appendix C. There is a trade-off between the reduction of noise (better for larger  $\sigma$ ) and resolution in the frequency space (better for smaller  $\sigma$ ). In this paper, we choose  $\sigma = 100$ , which corresponds to the resolution  $\sigma^{-1} \approx 0.01$  in the frequency space.

ESR spectra  $I(\omega)$  obtained numerically are shown in Fig. 5 for  $S = 10$ , and in Fig. 6 for  $S = 2$ . They are related to the spectrum discussed in Fig. 4 via eqs. 25 and 30. We note that  $I(\omega')$  at  $\omega' \sim 0$  is suppressed by the factor  $\omega'^2$  compared to  $|\langle L_T^+ L_T^- \rangle|(\omega')$ .

The dependence on the spin quantum number  $S$  comes only through the effective coupling constant  $g_R$ , as given by eqs. (35) and (5). From Fig. 5 and Fig. 6, we can see

that resonance splits to two peaks as  $h$  is increased. One peak at  $\omega \approx H$  results from the paramagnetic resonance. The intensity of this absorption peak becomes smaller as the staggered field becomes larger. For  $S = 10$ , the second peak at higher frequency is sharp, while the original paramagnetic peak at  $\omega' \approx H'$  is almost invisible except for  $h' = 0.5 \times 10^{-3}$ . On the other hand, for  $S = 2$ , the original paramagnetic peak persists and the second peak is very broad for the studied parameter range.

The second peak at higher frequency  $\omega > H$  must be caused by the staggered magnetic field, because it becomes dominant while the paramagnetic resonance peak is suppressed, as we increase the staggered field. As we increase  $S$ , this peak survives while the paramagnetic resonance vanishes as shown in Fig. 5. In the next section, we will discuss the physical origin of the new peak at  $\omega > H$ , as well as the difference between  $S = 10$  (Fig. 5) and  $S = 2$  (Fig. 6). The shape of each peak is asymmetric, suggesting that the lineshape is not a simple Lorentzian, in contrast to many cases with strong exchange interactions.<sup>1,2,15</sup>

We note that the location of the paramagnetic peak in Fig. 6 is at  $\omega' \approx 0.015$  which is higher than expected  $H' = 0.005$ . This is an artifact due to the windowing (64), as discussed in Appendix C.

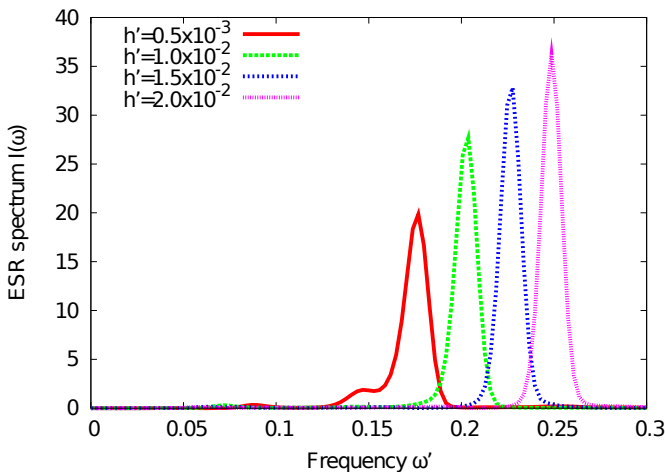


FIG. 5. ESR spectra for the  $S = 10$  case. We use dimensionless parameters  $T' = 0.3$ ,  $H' = 0.15$ . While the paramagnetic resonance peak vanishes for  $h' \geq 1.5 \times 10^{-2}$ , the peak in high frequency side survives. The high-frequency peak is much sharper compared to the corresponding resonance in the  $S = 2$  case (Fig. 6).

## V. SPIN WAVE THEORY

We propose an antiferromagnetic spin wave theory in order to explain the second peak at higher frequency ob-

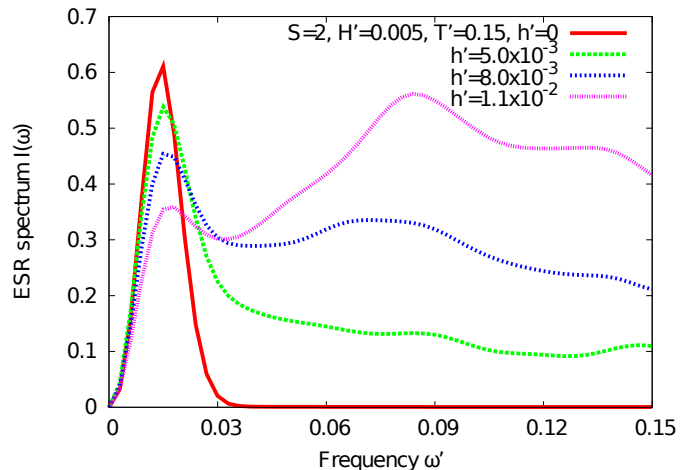


FIG. 6. ESR spectra for the dimensionless staggered field  $h' = h/2JS = 0, 5.0 \times 10^{-3}, 8.0 \times 10^{-3}$  and  $1.1 \times 10^{-2}$  are shown. Here we assume  $S = 2$ . The dimensionless uniform field and temperature are respectively given as  $H' = H/2JS = 0.005$  and  $T' = T/2JS = 0.15$ . In addition to the paramagnetic resonance ( $h' = 0$ ) at  $\omega \approx H$ , we can observe the very broad peak in higher frequency side.

served in Figs. 5 and 6. Here we discuss linearized fluctuations around the antiferromagnetic order externally imposed by the staggered field. In this aspect, it is distinguished from the standard theory of antiferromagnetic resonance, in which the antiferromagnetic order is caused by a spontaneous symmetry breaking.

We initiate our discussion by taking the Lagrangian in the large  $h$  regime, which is (21), because the additional peak originate in the large  $h$  limit  $h \rightarrow +\infty$ . By replacing the bare parameters to the renormalized ones, we obtain the classical spin wave theory:

$$\mathcal{H}'_{\text{cl}} = \frac{1}{2g_R(T)} \left[ (\partial_t \mathbf{m})^2 + (\partial_x \mathbf{m})^2 + \Delta_y'^2 (m^y)^2 + \Delta_z'^2 (m^z)^2 \right] \quad (65)$$

This Hamiltonian indicates that the classical spin dynamics in the large  $h$  limit is governed by the two harmonic modes  $m^y$  and  $m^z$ . These oscillating modes have the eigenfrequencies (22) and (23).

Now let us discuss the condition for the spin-wave theory to be justified. The spin-wave theory is based on the assumption that the field  $\mathbf{n}$  is polarized along the staggered field direction, and the fluctuation around the polarized groundstate is small. Therefore, the condition can be written as

$$(m^y)^2 + (m^z)^2 \ll 1. \quad (66)$$

Since  $\Delta_z' > \Delta_y'$  for any  $h'$ , we can expect  $\langle (m^z)^2 \rangle < \langle (m^y)^2 \rangle$ . Thus, it is sufficient to require  $\langle (m^y)^2 \rangle \ll 1$ . The Gaussian Hamiltonian (65) leads

$$\langle (m^y)^2 \rangle \approx g_R(T) T' \frac{1}{2\Delta_y'} \ll 1$$

and this immediately results in

$$T' \ll \frac{2}{g_R(T)} \Delta'_h \quad (67)$$

In terms of the physical staggered field  $h$ , this condition can be written as eq. (46).

We note that, the classical approach requires (6), namely

$$T' \gg \max(\Delta', \Delta'_h, H'). \quad (68)$$

In particular,  $T' \gg \Delta'_h$  is required. In the classical limit  $S \rightarrow \infty$ , the renormalized coupling constant  $g_R(T)$  approaches zero. This indicates that the temperature range, where both (67) and (68) hold, becomes larger as we increase the spin quantum number  $S$ .

In the classical picture, ESR corresponds to precession of magnetic moments. If there is no anisotropic interaction, the *total* magnetic moment  $\mathbf{L}_T$  precesses around the field  $\mathbf{H}$  with the frequency  $\omega = H$  without any dissipation. The modes mentioned above seem to affect the dynamics of  $\mathbf{L}_T$  through the equation of motion (62). The additional peak reflects the eigenfrequency of  $\mathbf{m}$  which is different from the paramagnetic resonance frequency  $H$ .

In order to see this, the following identity on the dynamical susceptibility  $\chi_{+-}(\omega)$  is useful:

$$\chi_{+-}(\omega) = \frac{2\langle L_T^z \rangle}{\omega - H} - \frac{\langle [\mathcal{A}, L_T^-] \rangle}{(\omega - H)^2} + \chi_{\mathcal{A}^\dagger \mathcal{A}}(\omega), \quad (69)$$

where  $\mathcal{A} = \Delta'_h n_T^z / g_R(T)$ . This formula is easily obtained by integrating the left hand side by parts. First and second terms in the right hand side have a singularity only at  $\omega = H$ . The last term  $\chi_{\mathcal{A}^\dagger \mathcal{A}}$  in (69) contributes to the additional singularity in  $\chi_{+-}''$ .

The dynamical correlation function of  $n^z$  can be easily calculated within the effective spin-wave Hamiltonian (65). Thus the spin-wave approximation predicts an additional resonance at the frequency identical to eq. (22),

$$\omega' = \Delta_{z'} = \sqrt{H'^2 + \Delta'_h{}^2}. \quad (70)$$

Let us compare this with the numerical results in Figs. 5 and 6. We note that, Figs. 5 and 6 are shown for  $\omega' < T'$ , where the classical approximation would work.

First we discuss the  $S = 10$  case, which is highly classical. The resonance peak observable in Fig. 5 for non-zero  $h'$  can be identified with the antiferromagnetic spin-wave resonance discussed above, since the original paramagnetic resonance peak disappears. The resonance frequencies for several values of  $h'$  are plotted in Fig. 7, and compared with the theoretical prediction (70). Both conditions (67) and (68) are satisfied in the cases studied in Fig. 7. Thus the linear spin-wave approximation of the classical O(3) NLSM should be valid. In fact, we find a very good agreement with the spin-wave theory prediction in this case.

The disappearance of the paramagnetic peak and the sharp spin-wave resonance corresponding to eq. (70) may be understood as consequences of small fluctuation around the polarized state along the staggered field. For a large spin such as  $S = 10$ , the coupling constant  $g_R$  is small and thus eq. (67) is easily satisfied, leading to small fluctuation (66). Thus the spectrum is well described by the spin-wave theory which gives the sharp resonance at frequency (70). The original paramagnetic resonance at  $\omega \sim H$  corresponds to global precession of spins around the magnetic field  $H \parallel z$ . When eq. (67) holds, the spins are polarized along the staggered field and thus the global precession cannot occur; the paramagnetic resonance is expected to vanish. This is consistent with the observed behavior in Fig. 5.

Next we discuss the  $S = 2$  case, in which the quantum fluctuations are stronger corresponding to the larger value of  $g_R$ . In this case, as we have seen in Fig. 6, two peaks are observed. The lower frequency peak represents the paramagnetic resonance at  $\omega \sim H$ , which is almost independent of the staggered field. As in the  $S = 10$  case, the higher frequency peak would be identified with the antiferromagnetic spin-wave. However, in this case, a quantitative analysis of the resonance frequency is not possible because the peak is very broad. The survival of the paramagnetic peak and the broadness of the antiferromagnetic spin-wave resonance for  $S = 2$  are consequences of large fluctuation owing to large  $g_R$ , in contrast to the  $S = 10$  case discussed above.

We note that, at a lower temperature, the fluctuation around the polarized state becomes smaller and the spin-wave theory holds better. However, for  $S = 2$ , the classical approximation is no longer valid in this regime. Nevertheless, the antiferromagnetic spin-wave resonance should exist also in the quantum regime; in fact, it exists even in the  $S = 1$  chain with a staggered field at low temperature<sup>10,11</sup>. Our classical calculation describes the broadening of the antiferromagnetic resonance at higher temperatures.

Finally, we note that, our theory predicts the spin-wave resonance frequency (22) to be independent of temperature. This is also in agreement with our numerical calculations (not shown). While the temperature-independence of the resonance frequency might seem obvious, it is owing to the lack of the renormalization of the staggered field for  $N = 3$  as shown in eq. (39). In a similar analysis based on the O( $N$ ) NLSM with  $N \geq 4$ , the “spin-wave” resonance frequency should depend on the temperature through the logarithmic correction.

## VI. SUMMARY AND DISCUSSION

We discussed ESR in the classical limit based on the O(3) NLSM and the corresponding CRM. Our discussion is valid in the classical temperature regime,

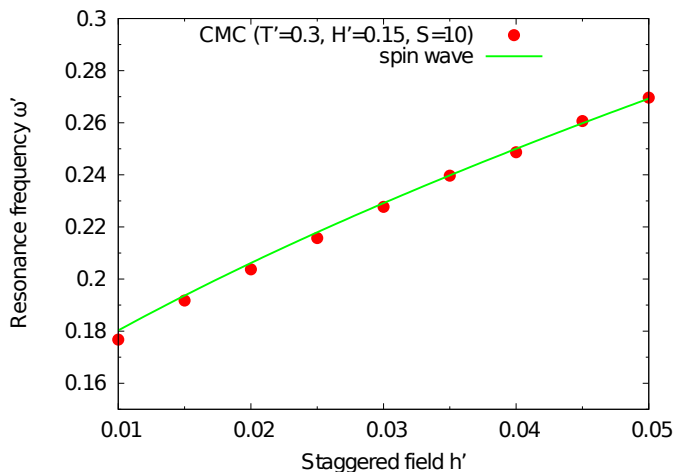


FIG. 7. Staggered field dependence of the resonance frequency in  $S = 10$  system at  $T' = 0.3, H' = 0.15$ . The results agree quite well with the prediction of the spin wave theory (70) (solid line). This implies that the resonance peak in the  $S = 10$  chain under a staggered field indeed corresponds to the antiferromagnetic spin wave.

$\max(\Delta, \Delta_h, H) \ll T \ll JS^2$ . Here the field theoretical picture by  $O(3)$  NLSM holds, and the system behaves classically. However the microscopic parameters in bare  $O(3)$  NLSM are renormalized by quantum fluctuations. The dynamics of the  $O(3)$  NLSM with renormalized parameters was then analyzed in the classical limit. Actual numerical calculations were done for the lattice version of the NLSM, namely the CRM.

We have demonstrated that numerically calculated ESR spectra show that the paramagnetic and antiferromagnetic resonance peaks coexist in this intermediate temperature regime. The latter is characteristic of this regime since it disappears in both lower and higher temperature regions. We analytically showed that the antiferromagnetic resonance frequency is  $\omega = \sqrt{H^2 + \Delta_h^2}$  based on the linearized spin wave-theory (65). This agrees well with the numerical results for a large spin quantum number  $S = 10$ . For  $S = 2$ , owing to larger fluctuation, the spin-wave theory is not quite justified in classical regime. Nevertheless, a broad resonance is observed in the spectrum, which is identified with the (remnant of) antiferromagnetic spin-wave resonance.

It is instructive to compare the present results with ESR in the  $S = 1/2$  antiferromagnetic chain. Although the  $S = 1/2$  chain at low temperature is described by a different theoretical approach (bosonization), as we have discussed in the Introduction, there is a qualitative similarity between the two cases. That is, the paramagnetic resonance at the frequency  $\omega \sim H$  is broadened and eventually disappears as the temperature is lowered. On the other hand, at lower temperatures, the new (antiferromagnetic resonance) peak at higher frequency becomes dominant.

There is an important difference in the frequency of the

antiferromagnetic resonance. In both cases, it is given by eq. (22). However, the staggered-field-induced gap has different dependence on the staggered field  $h$ . In general, the staggered-field-induced gap is given by

$$\Delta_h \propto h^{\frac{1}{2-\gamma}}, \quad (71)$$

where  $\gamma$  is the anomalous dimension of the staggered magnetization. For the low-energy limit of the  $S = 1/2$  chain, the staggered magnetization has the anomalous dimension  $1/2$ . Thus it follows<sup>15</sup> that

$$\Delta_h \propto h^{2/3}, \quad (72)$$

up to logarithmic corrections. In contrast, in the present case, the anomalous dimension is basically zero and thus

$$\Delta_h \propto h^{1/2}, \quad (73)$$

which is consistent with eq. (16). This difference can be understood as an effect of strong quantum fluctuations in the  $S = 1/2$  chain at low temperatures, on the antiferromagnetic resonance<sup>20,21</sup>.

The lineshape of each peak in the present system appears to be asymmetric and thus non-Lorentzian. This would also be a significant difference from the  $S = 1/2$  case, in which the broadening of the paramagnetic peak has Lorentzian form.<sup>15</sup>

In order to apply the present formulation to quantum spin systems, we need  $S \geq 2$  in the case of a single chain. The temperature range  $\max(\Delta, \Delta_h, H) \ll T \ll JS^2$  is not wide enough for the  $S = 1$  chains. For the  $S = 2$  Heisenberg antiferromagnetic chain, we confirmed the validity of the classical  $O(3)$  NLSM approach in a finite magnetic field by calculating the magnetization density with quantum Monte Carlo simulations. The results show a good agreement with the effective classical  $O(3)$  NLSM.

We thus expect that our approach is applicable to the  $S = 2$  Haldane chain compound  $\text{MnCl}_3(\text{bpy})$ , which may bear an effective staggered field due to its staggered crystal structure. It would be interesting to measure ESR spectrum and compare to our prediction, especially the appearance of the antiferromagnetic resonance and its broadening. The present results can also be applied to spin ladders or tubes, if the system is described by the classical  $O(3)$  NLSM, and if the staggered field is unfrustrated as in eq. (8).

Finally, let us comment on extension of the present approach to ESR in 2 dimensional antiferromagnets. The present approach can be extended to 2 dimensions, as discussed in the Introduction. The temperature range for the classical approach is wider in 2 dimensions, as it is not limited from below by the Haldane gap. This is favorable for the classical approach in 2 dimensions. On the other hand, the increase of the computational cost in higher dimensions may be a problem for calculation of ESR spectra which requires high precision and resolution. Since ESR in 2 dimensional systems is rather

little understood, it would be interesting to pursue this approach in 2 dimensions. We plan to attempt this as a next step.

### ACKNOWLEDGEMENT

This work is supported in part by Global COE Program “The Physical Sciences Frontier”, MEXT, Japan (S.C.F.), JSPS Grant-in-Aid for Scientific Research (KAKENHI) Nos. 18540341 and 21540381 (S.C.F. and M.O.), NSERC and CIFAR (I.A.). Part of the numerical calculations were performed at the ISSP Supercomputer Center of the University of Tokyo. We thank Masayuki Hagiwara for useful discussions, and the ALPS project for providing quantum Monte Carlo simulation code used in this work.

### Appendix A: Proof of (58)

Let us define the partition function

$$Z(\mathbf{H}) = \int \mathcal{D}\mathbf{n}\mathcal{D}\mathbf{L} \prod_x \delta(\mathbf{n}(x) \cdot \mathbf{L}(x)) \delta(\mathbf{n}^2(x) - 1) e^{-\mathcal{H}/T} \quad (\text{A1})$$

The key observation is that, thanks to the rotation invariance of the Hamiltonian, the partition function depends just on the length of  $\mathbf{H}$ , namely  $Z(\mathbf{H}) = Z(|\mathbf{H}|)$ . Let us consider the two infinitesimal variations of  $\mathbf{H}$  from  $\mathbf{H}_0 = (0, 0, H_0)$ . The first variation is  $\mathbf{H} = (0, 0, H_0 + \delta H)$ . The partition function can be expanded in terms of  $\delta H$  as

$$Z(\mathbf{H}) = Z(H_0) \left( 1 + \frac{1}{T} \langle L_T^z \rangle_0 \delta H \right) + O((\delta H)^2), \quad (\text{A2})$$

up to the first order in  $\delta H$ . Here  $\langle \cdot \rangle_0$  means that the expectation value with  $\mathbf{H} = \mathbf{H}_0$ . The second variation we consider is  $\mathbf{H} = (\delta H', 0, H_0)$ . Again the partition function can be expanded in terms of  $\delta H'$ . The first order term actually vanishes here because  $\langle L_T^x \rangle_0 = 0$  due to the symmetry. The expansion up to the second order is

$$Z(\mathbf{H}) = Z(H_0) \left( 1 + \frac{1}{2T^2} \langle (L_T^x)^2 \rangle_0 (\delta H')^2 \right) + O((\delta H')^3). \quad (\text{A3})$$

We compare the variation of  $\mathbf{H}$  by the two infinitesimal variation of  $\mathbf{H}$ .  $|\mathbf{H}| \approx H_0 + \delta H$  for the first variation and  $|\mathbf{H}| \approx H_0 + (\delta H')^2/2H_0$  for the second. The isotropy of the partition function (A1) leads that  $\delta H = (\delta H')^2/2H_0$ . Thus, we find the identity

$$\langle (L_T^x)^2 \rangle_0 = \frac{T}{H_0} \langle L_T^z \rangle_0, \quad (\text{A4})$$

which is valid for any temperature and for any magnetic field  $H_0$ . This result (A4) is nothing but (58).

### Appendix B: Numerical methods

Our numerical computation of the classical dynamics consists of two steps: preparing the initial states at equilibrium, and solving the equations of motion numerically from the initial state.

#### 1. Initial states at equilibrium

The initial states are generated by the Monte Carlo method as follows. This method is also used to study static properties in Sec. III C. For the sake of simplicity, we will discuss in terms of continuum variables for simplicity. The actual calculation is done for the CRM on a lattice, for which  $(\partial_x \mathbf{n}_j)^2$  is to be replaced by  $-\frac{2}{b^2} \mathbf{n}_j \cdot \mathbf{n}_{j+1}$ .

First we eliminate  $\mathbf{L}$  from the classical Hamiltonian (54). For simplicity, we denote  $\mathbf{n}(t=0, x)$  and  $\mathbf{L}(t=0, x)$  as  $\mathbf{n}_0(x)$  and  $\mathbf{L}_0(x)$  respectively. The constraint  $\mathbf{n}_0 \cdot \mathbf{L}_0 = 0$  decrease the degrees of freedom of  $\mathbf{L}_0$ . For instance, we eliminate  $L_0^z$  from the Hamiltonian,

$$\begin{aligned} \mathcal{H}'_{\text{cl}} &= \frac{1}{2g_R(T)} (\partial_x \mathbf{n}_0)^2 + \frac{g_R(T)}{2} \mathbf{L}_0^2 - H' L_0^z - \frac{2h'}{g_R(T)} n_0^x \\ &= \frac{1}{2g_R(T)} (\partial_x \mathbf{n}_0)^2 + \frac{g_R(T)}{2} \left[ (\mathbf{L}_0^\perp)^2 + \frac{(\mathbf{n}_0^\perp \cdot \mathbf{L}_0^\perp)^2}{(n_0^z)^2} \right] \\ &\quad + H' \frac{\mathbf{n}_0^\perp \cdot \mathbf{L}_0^\perp}{n_0^z} - \frac{2h'}{g_R(T)} n_0^x, \end{aligned}$$

where  $\mathbf{L}_0^\perp$  and  $\mathbf{n}_0^\perp$  are defined as  $\mathbf{L}_0^\perp \equiv (L_0^x, L_0^y, 0)$  and  $\mathbf{n}_0^\perp = (n_0^x, n_0^y, 0)$  respectively.  $\mathbf{L}_0^\perp$  is distributed with Gaussian distribution with an average  $-\chi_{u\perp} H \mathbf{n}_0^\perp n_0^z$ , and the variance  $T\chi_{u\perp}$ . We can integrate out  $\mathbf{L}_0^\perp$  because the Hamiltonian is harmonic in  $\mathbf{L}_0^\perp$ .

$$\mathcal{H}'_{\text{eff}} = \frac{1}{2g_R(T)} (\partial_x \mathbf{n}_0)^2 + \frac{H'^2}{2g_R(T)} (n_0^z)^2 - \frac{2h'}{g_R(T)} n_0^x \quad (\text{B1})$$

Starting from an arbitrary configuration of  $\{\mathbf{n}(x)\}$ , we thermalize it by classical Monte Carlo method based on the Wolff algorithm<sup>34</sup>.  $\mathbf{L}_0^\perp$  is calculated by  $\mathbf{L}_0^\perp = -H' \mathbf{n}_0^\perp n_0^z / g_R(T) + \mathbf{R}$ .  $\mathbf{R}$  is a random vector whose distribution is Gaussian with an average 0 and a variance  $T\chi_{u\perp}$ . The constraint  $\mathbf{n}_0 \cdot \mathbf{L}_0 = 0$  determines  $\langle L_0^z \rangle$ .

#### 2. Calculation of dynamical correlation functions

We need to solve the classical equations of motion (62) and (63) numerically with the initial states produced in Appendix B. We should pay attention to the conserved quantities, the total energy and the uniform magnetization (if there is no staggered field) in our system. Ordinary numerical methods for solving the equations motion, for instance, Runge-Kutta method or the predictor-corrector method, result in the violation of the conservation law. This violation is caused by discretizations.

Even if the continuum equations of motion preserve the conservation laws, the discretized version of the equations of motion do not necessarily preserve them.

This problem is serious in our situation. ESR spectrum requires asymptotic behavior of the dynamical correlation function, namely  $\langle L_{\top}^+(t)L_{\top}^-(0) \rangle$  at  $t \rightarrow +\infty$ . The configuration  $\{\mathbf{n}(t, x), \mathbf{L}(t, x)\}$  may be far from the real one which exactly conserves the energy once the conservation law is violated.

#### a. Symplectic methods

We overcame this difficulty by applying ‘‘symplectic’’ methods<sup>29,30</sup>. This algorithm is based on the Suzuki-Trotter decomposition<sup>35,36</sup> of integrators. Applications to classical spin systems are explained in detail in Refs. 29 and 30.

Let us consider the time evolution of a scalar  $f(t)$  for simplicity. We assume the equation of motion for  $f(t)$  as

$$\frac{df}{dt} = \mathcal{F}(f(t)) = \mathcal{F}_1(f(t)) + \mathcal{F}_2(f(t)).$$

Further we assume that we can exactly solve the equations

$$\frac{df}{dt} = \mathcal{F}_i(f) \quad (\text{B2})$$

for  $i = 1, 2$ . Infinitesimal time evolution of  $f$  from  $t$  to  $t + \delta t$  has an exponential form

$$f(t + \delta t) = e^{\delta t \mathfrak{h}} f(t) = e^{\delta t (\mathfrak{h}_1 + \mathfrak{h}_2)} f(t). \quad (\text{B3})$$

Since we can solve (B2) exactly, we know the explicit form of  $\mathfrak{h}_1$  and  $\mathfrak{h}_2$  and thus,  $e^{\delta t \mathfrak{h}_1}$  and  $e^{\delta t \mathfrak{h}_2}$ . The essence of the symplectic method is in approximating the operator  $e^{\delta t (\mathfrak{h}_1 + \mathfrak{h}_2)}$  by exactly known operators  $e^{\delta t \mathfrak{h}_1}$  and  $e^{\delta t \mathfrak{h}_2}$ .

The fourth order approximation<sup>37</sup> is known:

$$e^{\delta t (\mathfrak{h}_1 + \mathfrak{h}_2)} = \prod_{i=1}^5 e^{p_i \delta t \mathfrak{h}_1 / 2} e^{p_i \delta t \mathfrak{h}_2} e^{p_i \delta t \mathfrak{h}_1 / 2}, \quad (\text{B4})$$

where  $p_1 = p_2 = p_4 = p_5 = 1/(4 - 4^{1/3})$  and  $p_3 = -4^{1/3}/(4 - 4^{1/3})$ . We can extend the decomposition (B4) to  $2n$ th order one with  $n \geq 3$ . By applying Baker-Campbell-Hausdorff (BCH) formula repeatedly, we can show that the right hand side in (B4) is  $e^{\delta t \mathfrak{h} + \mathcal{O}((\delta t)^6)}$ . It is easily proved that  $2n$ -th order decomposition of this type is  $(2n + 1)$ -th order approximation. It follows immediately that the symplectic method is more accurate than other naive methods and that the conserved quantities during the calculation do not deviate from the exact value. Let us discuss a specific example about the latter. In Hamilton systems, the operator  $\mathfrak{h}$  is the Hamiltonian itself. Let us write the approximated  $\mathfrak{h}$  in (B4) as  $\mathfrak{h}_4$ . The difference  $\mathfrak{h}_4 - \mathfrak{h}$  is bounded as

$$\mathfrak{h}_4 - \mathfrak{h} = \text{const.} \times (\delta t)^5 \quad (\text{B5})$$

according to (B4) and BCH formula. (B5) is much more accurate than that of 4th order Runge-Kutta method. Let us consider the total energy at time  $t$  and denote it as  $E(t)$ . First we prepare initial state and fix  $E(t = 0)$ . By applying the symplectic method,  $E(t) - E(0)$  is order of  $(\delta t)^5$ , thus,  $E(t) - E(0) \sim (\delta t)^5$ . However, by the Runge-Kutta method, the error is increasing at least linearly with respect to  $t$ . Thus,  $E(t) - E(0) \sim t$  becomes quite large if we want to consider large  $t$ .

Thus, if we apply the symplectic method, the total energy conserves with high accuracy during the discretized time evolution.

#### b. Application to classical rotor model

The application of this symplectic method is as follows. We decompose the equations of motion (62) and (63):

$$\begin{cases} \partial_{t'} \mathbf{n}_j = g_R(T) \mathbf{L}_j \times \mathbf{n}_j \\ \partial_{t'} \mathbf{L}_j = 0 \end{cases} \quad (\text{B6a})$$

$$\begin{cases} \partial_{t'} \mathbf{n}_j = -\mathbf{H}' \times \mathbf{n}_j \\ \partial_{t'} \mathbf{L}_j = -\mathbf{H}' \times \mathbf{n}_j \end{cases} \quad (\text{B6b})$$

$$\begin{cases} \partial_{t'} \mathbf{n}_j = 0 \\ \partial_{t'} \mathbf{L}_j = \frac{1}{b^2 g_R(T)} \mathbf{n}_j \times (\mathbf{n}_{j+1} + \mathbf{n}_{j-1}) \frac{2h'}{g_R(T)} \mathbf{e}_x \times \mathbf{n}_j \end{cases} \quad (\text{B6c})$$

Each of these equations are exactly solvable. For instance, (B6a) is solved as follows:

$$\begin{aligned} \mathbf{n}_j(t' + \delta t') &= \mathbf{n}_j(t') \cos(g_R(T) \delta t' |\mathbf{L}_j(t)|) \\ &\quad + \frac{\mathbf{L}_j(t') \times \mathbf{n}_j(t')}{|\mathbf{L}_j(t')|} \sin(g_R(T) \delta t' |\mathbf{L}_j(t)|) \\ \mathbf{L}_j(t' + \delta t') &= \mathbf{L}_j(t') \end{aligned}$$

We consider this step from  $t'$  to  $t' + \delta t'$  as  $e^{\delta t' A}$ . In the same way we define the time step  $e^{\delta t' B}$  and  $e^{\delta t' C}$  as

$$\begin{aligned} \mathbf{n}_j(t' + \delta t') &= \mathbf{n}_j(t') \cos(H \delta t') - \frac{\mathbf{H}' \times \mathbf{n}_j(t')}{H'} \sin(H \delta t') \\ \mathbf{L}_j(t' + \delta t') &= \mathbf{L}_j(t') \cos(H \delta t') - \frac{\mathbf{H}' \times \mathbf{L}_j(t')}{H'} \sin(H \delta t') \end{aligned}$$

and

$$\begin{aligned} \mathbf{n}_j(t' + \delta t') &= \mathbf{n}_j(t') \\ \mathbf{L}_j(t' + \delta t') &= \mathbf{L}_j(t') + \delta t' \left( \frac{1}{g_R(T)} \mathbf{n}_j(t') \right. \\ &\quad \left. \times (\mathbf{n}_{j+1}(t') + \mathbf{n}_{j-1}(t')) - \frac{2h'}{g_R(T)} \mathbf{e}_x \times \mathbf{n}_j(t') \right) \end{aligned}$$

respectively. Actual time evolution is considered as  $e^{\delta t'(A+B+C)}$ . Second order decomposition of  $e^{\delta t'(A+B+C)}$  is  $e^{\delta t'(A+B+C)} = e^{\delta t' A/2} e^{\delta t' B/2} e^{\delta t' C} e^{\delta t' B/2} e^{\delta t' C/2}$ . In this manner, we can apply these to the symplectic method. Fourth order calculation conserve the total energy within the precision  $\Delta E/E \lesssim 10^{-8}$ .

### Appendix C: Effects of windowing

In this Appendix, we discuss reduction of white noise by windowing. For simplicity, here we identify time  $t$  and frequency  $\omega$  with the rescaled variables  $t'$  and  $\omega'$ .

In general, the Fourier transform of a real-time function  $f(t)$  is defined by

$$F(\omega) = \int dt f(t) e^{i\omega t} \quad (\text{C1})$$

From the definition, Parseval's identity

$$\int \frac{d\omega}{2\pi} |F(\omega)|^2 = \int dt |f(t)|^2, \quad (\text{C2})$$

follows. In practice, we use  $f(t)$  at discrete time with time step  $\Delta t$  and upper bound  $t_{\max}$ . In this case, the integrals are replaced by discrete sums

$$\int dt \rightarrow \Delta t \sum_{0 \leq n < t_{\max}/\Delta t}, \quad (\text{C3})$$

$$\int \frac{d\omega}{2\pi} \rightarrow \frac{1}{t_{\max}} \sum_{0 \leq m < t_{\max}/\Delta t}. \quad (\text{C4})$$

Assuming white noise, we consider the case  $|f_{\text{noise}}(t)|^2 = \delta^2$  at any discrete time and  $|F_{\text{noise}}(\omega)|^2$  is independent of frequency  $\omega$ . Then Parseval's identity implies

$$|F_{\text{noise}}(\omega)|^2 = \delta^2 t_{\max} \Delta t. \quad (\text{C5})$$

Namely, the white noise in the frequency space increases as the sampling time interval  $t_{\max}$  is increased. The white noise could be reduced simply by taking smaller interval  $t_{\max}$ , but it enhances spectral leakage. A better alternative is to use the window function with smaller width, effectively reducing the sampling time interval. In this paper, we use the Gaussian window function. The Fourier

transform with the windowing is defined as

$$\tilde{F}(\omega) \equiv \int dt f(t) e^{-t^2/(2\sigma^2)} e^{i\omega t}. \quad (\text{C6})$$

The counterpart of eq. (C2) becomes

$$\int \frac{d\omega}{2\pi} |\tilde{F}(\omega)|^2 = \int dt |f(t)|^2 e^{-t^2/\sigma^2}. \quad (\text{C7})$$

For the white noise with  $|f_{\text{noise}}(t)|^2 = \delta^2$ , and we find

$$|\tilde{F}_{\text{noise}}(\omega)|^2 = \delta^2 \sqrt{\pi} \sigma \Delta t. \quad (\text{C8})$$

In our study,  $f_{\text{noise}}(t)$  corresponds to the noise in the dynamical correlation function  $\langle L_{\text{T}}^+(t) L_{\text{T}}^-(0) \rangle$ . sampling time step is  $\Delta t \sim 0.1$ , and  $\delta \sim 0.02$ . For  $\sigma = 100$ , this gives  $|\tilde{F}_{\text{noise}}(\omega)| \sim 0.2$ , which is about 2 % of the observed signal. In other words, this signal-to-noise ratio is achieved with  $\sigma = 100$ .

On the other hand, there is a side-effect of the windowing. In the absence of the staggered field  $h' = 0$ , the exact spectrum is proportional to  $\delta(\omega - H)$ , according to the general result in the absence of anisotropy. However, in Fig. 6, the paramagnetic resonance appears to have a finite width and the peak seems to be shifted to higher frequency  $\omega' \approx 0.015$  from the expected  $\omega' = H' = 0.005$ .

This is actually due to the the artificial linewidth  $\sigma^{-1}$  introduced through the window function (64). It actually dominates the linewidth of the paramagnetic peak in Fig. 6. Once a finite width is induced, the peak in the dynamical susceptibility is distorted by the factor  $1 - e^{-\omega/T}$  (which is proportional to  $\omega$  at low frequency and give more weights to higher frequencies) in the definition, eq. (30). For a uniform field  $H'$  sufficiently larger than the resolution, we find the (resolution-limited) paramagnetic resonance peak at  $\omega' \sim H'$ , as expected. In Fig. 6, we have shown the data for small  $H'$  so that the additional broad peak can be observable in a wide range of frequency within the validity of the classical approximation. The low-frequency peak in Fig. 6 is smoothly connected to the paramagnetic resonance peak at  $\omega' \sim H'$ , when the uniform magnetic field  $H'$  is increased; thus it can be identified with the paramagnetic resonance peak despite the apparent width and shift due to the frequency resolution in the calculation. In fact, the paramagnetic peak itself can be observed with a larger value of  $\sigma$ .

<sup>1</sup> R. Kubo and K. Tomita, J. Phys. Soc. Jpn **9**, 888 (1954).

<sup>2</sup> H. Mori and K. Kawasaki, Prog. Theor. Phys. **28**, 971 (1962).

<sup>3</sup> S. Chakravarty, B. I. Halperin, and D. R. Nelson, Phys. Rev. B **39**, 2344 (1989).

<sup>4</sup> S. Tyč, B. I. Halperin, and S. Chakravarty, Phys. Rev. Lett. **62**, 835 (1989).

<sup>5</sup> K. Damle and S. Sachdev, Phys. Rev. B **57**, 8307 (1998).

<sup>6</sup> C. Buragohain and S. Sachdev, Phys. Rev. B **59**, 9285

(1999).

<sup>7</sup> I. Affleck, Phys. Rev. B **41**, 6697 (1990).

<sup>8</sup> H. Huang and I. Affleck, Phys. Rev. B **69**, 184414 (2004).

<sup>9</sup> S. Todo and K. Kato, Phys. Rev. Lett. **87**, 047203 (2001).

<sup>10</sup> T. Sakai and H. Shiba, J. Phys. Soc. Jpn **63**, 867 (1994).

<sup>11</sup> P. P. Mitra and B. I. Halperin, Phys. Rev. Lett. **72**, 912 (1994).

<sup>12</sup> M. Oshikawa and I. Affleck, Phys. Rev. Lett. **79**, 2883 (1997).

- <sup>13</sup> A. Meyer, A. Gleizes, J. Girerd, M. Verdaguer, and O. Kahn, *Inorg. Chem* **21**, 1729 (1982).
- <sup>14</sup> M. Date, H. Yamazaki, M. Motokawa, and S. Tazawa, *Progress of Theoretical Physics Supplement* **46**, 194 (1970).
- <sup>15</sup> M. Oshikawa and I. Affleck, *Phys. Rev. Lett.* **82**, 5136 (1999).
- <sup>16</sup> M. Oshikawa and I. Affleck, *Phys. Rev. B* **65**, 134410 (2002).
- <sup>17</sup> G. E. Granroth, M. W. Meisel, M. Chaparala, T. Jolicœur, B. H. Ward, and D. R. Talham, *Phys. Rev. Lett.* **77**, 1616 (1996).
- <sup>18</sup> M. Sato and M. Oshikawa, *Phys. Rev. B* **69**, 054406 (2004).
- <sup>19</sup> J. Zhao, X. Wang, T. Xiang, Z. Su, L. Yu, J. Lou, and C. Chen, *Phys. Rev. B* **73**, 012411 (2006).
- <sup>20</sup> T. Nagamiya, *Progress of Theoretical Physics* **6**, 342 (1951).
- <sup>21</sup> F. Keffer and C. Kittel, *Phys. Rev.* **85**, 329 (1952).
- <sup>22</sup> T. Iitaka and T. Ebisuzaki, *Phys. Rev. Lett.* **90**, 047203 (2003).
- <sup>23</sup> E. Brézin and J. Zinn-Justin, *Phys. Rev. B* **14**, 3110 (1976).
- <sup>24</sup> I. Affleck, D. Gepner, H. J. Schulz, and T. Ziman, *J. Phys. A:Math. Gen.* **22**, 511 (1989).
- <sup>25</sup> M. E. Fisher, *Am. J. Phys.* **32**, 343 (1964).
- <sup>26</sup> Y. Kim, M. Greven, U.-J. Wiese, and R. Birgeneau, *Eur. Phys. J. B* **4**, 291 (1998).
- <sup>27</sup> F. Alet, P. Dayal, A. Grzesik, A. Honecker, M. Koerner, A. Laeuchli, S. R. Manmana, I. P. McCulloch, F. Michel, R. M. Noack, et al., *J. Phys. Soc. Jpn. Suppl.* **74**, 30 (2005).
- <sup>28</sup> A. Albuquerque, F. Alet, P. Corboz, P. Dayal, A. Feiguin, S. Fuchs, L. Gamper, E. Gull, S. Gürtler, A. Honecker, et al., *J. Magn. Magn. Mater.* **310**, 1187 (2007).
- <sup>29</sup> M. Krech, A. Bunker, and D. P. Landau, *Comput. Phys. Commun.* **111**, 1 (1998).
- <sup>30</sup> D. P. Landau, A. Bunker, H. G. Evertz, M. Krech, and S. Tsai, *Prog. Theor. Phys. Suppl.* **138**, 423 (2000).
- <sup>31</sup> J. Arrillaga and N. R. Watson, *power system harmonics* (John Wiley & Sons Ltd., 2003).
- <sup>32</sup> K. Chen and D. P. Landau, *Phys. Rev. B* **49**, 3266 (1994).
- <sup>33</sup> H. G. Evertz and D. P. Landau, *Phys. Rev. B* **54**, 12302 (1996).
- <sup>34</sup> U. Wolff, *Phys. Rev. Lett.* **62**, 361 (1989).
- <sup>35</sup> M. Suzuki, *Phys. Lett. A* **146**, 319 (1990).
- <sup>36</sup> M. Suzuki, *Phys. Lett. A* **165**, 387 (1992).
- <sup>37</sup> H. Yoshida, *Phys. Lett. A* **150**, 262 (1990).